



Article

The Antiviral Effect of *Isatis* Root Polysaccharide against NADC30-like PRRSV by Transcriptome and Proteome Analysis

Dike Jiang ^{1,†} , Ling Zhang ^{2,†}, Guangheng Zhu ¹, Pengfei Zhang ¹, Xulong Wu ³, Xueping Yao ¹, Yan Luo ¹, Zexiao Yang ¹, Meishen Ren ¹, Xinping Wang ^{2,*}, Sheng Chen ⁴  and Yin Wang ^{1,*}

- ¹ Key Laboratory of Animal Diseases and Human Health of Sichuan Province, College of Veterinary Medicine, Sichuan Agricultural University, Chengdu 611130, China; 2020103005@stu.sicau.edu.cn (D.J.); 2018303051@stu.sicau.edu.cn (G.Z.); 2018103006@stu.sicau.edu.cn (P.Z.); 13577@sicau.edu.cn (X.Y.); 41187@sicau.edu.cn (Y.L.); 13643@sicau.edu.cn (Z.Y.); 14773@sicau.edu.cn (M.R.)
- ² College of Veterinary Medicine, Jilin University, Changchun 130012, China; zhangl15@mails.jlu.edu.cn
- ³ Branch of Animal Husbandry and Veterinary Medicine, Chengdu Agricultural College, Chengdu 611130, China; yaanwuxl@163.com
- ⁴ Department of Infectious Diseases and Public Health, Jockey Club College of Veterinary Medicine and Life Sciences, City University of Hong Kong, Hong Kong 999077, China; shechen@cityu.edu.hk
- * Correspondence: drxwang@jlu.edu.cn(X.W.); 10334@sicau.edu.cn (Y.W.)
- † These authors contributed equally to this work.



Citation: Jiang, D.; Zhang, L.; Zhu, G.; Zhang, P.; Wu, X.; Yao, X.; Luo, Y.; Yang, Z.; Ren, M.; Wang, X.; et al. The Antiviral Effect of *Isatis* Root Polysaccharide against NADC30-like PRRSV by Transcriptome and Proteome Analysis. *Int. J. Mol. Sci.* **2022**, *23*, 3688. <https://doi.org/10.3390/ijms23073688>

Academic Editor: Michele Costanzo

Received: 26 February 2022

Accepted: 25 March 2022

Published: 28 March 2022

Publisher's Note: MDPI stays neutral with regard to jurisdictional claims in published maps and institutional affiliations.



Copyright: © 2022 by the authors. Licensee MDPI, Basel, Switzerland. This article is an open access article distributed under the terms and conditions of the Creative Commons Attribution (CC BY) license (<https://creativecommons.org/licenses/by/4.0/>).

Abstract: (1) Background: In recent years, the porcine reproductive and respiratory syndrome virus (PRRSV) has become a virulent pathogen that has caused devastating diseases and economic losses worldwide in the swine industry. *IRPS* has attracted extensive attention in the field of virology. However, it is not clear that *IRPS* has an antiviral effect on PRRSV at gene and protein levels. (2) Methods: We used transcriptomic and proteomic analysis to investigate the antiviral effect of *IRPS* against PRRSV. Additionally, a microbiome was used to explore the effects of *IRPS* on gut microbes. (3) Results: *IRPS* significantly extenuated the pulmonary pathological lesions and inflammatory response. We used transcriptomic and proteomic analysis to investigate the antiviral effect of *IRPS* against PRRSV. In the porcine model, 1669 differentially expressed genes (DEGs) and 370 differentially expressed proteins (DEPs) were identified. Analysis of the DEG/DEP-related pathways indicated immune-system and infectious-disease (viral) pathways, such as the NOD-like receptor (NLR) signaling pathway, toll-like receptor (TLR) signaling pathway, and Influenza A-associated signaling pathways. It is noteworthy that *IRPS* can inhibit NLR-dependent gene expression, then reduce the inflammatory damage. *IRPS* could exert beneficial effects on the host by regulating the structure of intestinal flora. (4) Conclusions: The antiviral effect of *IRPS* on PRRSV can be directly achieved by omics techniques. Specifically, the antiviral mechanism of *IPRS* can be better elucidated by screening target genes and proteins using transcriptome and proteome sequencing, and then performing enrichment and classification according to DEGs and DEPs.

Keywords: *isatis* root polysaccharide; NADC30-like porcine reproductive and respiratory syndrome virus; transcriptomic and proteomic analysis

1. Introduction

Porcine reproductive and respiratory syndrome virus (PRRSV) is one of the most important causative pathogens of respiratory and reproductive diseases, severely impacting the global swine industry [1]. It is a single-stranded RNA virus. Its viral protein exhibits a high mutation rate, hindering innate immune response [2]. It is listed as a notified disease by the Office International des Epizooties (OIE) and as a type of disease in China [3]. The NADC30-like PRRSV strain is an NA-PRRSV (North American-like) that was isolated in the US in 2008 [4]. The NADC30-like stain has spread throughout China. Many researchers have found that NADC30-like PRRSV led to the re-emergence of new variants with different

virulence levels [5–7]. It has not only caused the outbreaks of clinical PRRS, but also participated in the recombination and generation of new strains of PRRSV, including recombination with HP-PRRSV (JXA1), classical PRRSV (CH-1a, VR2332), and attenuated vaccines (JXA1-P80, TJM-F92-like) [8–11].

Additionally, no effective vaccine has been invented for prevention and treatment in recent years. Vaccines sold in China mainly include the inactivated vaccine (CH-1a), classical attenuated vaccines (CH-1R, R98, VR2332), and HP-PRRSV vaccines (JXA1-R, HuN4-F112, TJM-F92, GDr180) [12–16]. Some large-scale pig farms in China are facilitating disease control instead of high-volume vaccination [17,18]. In clinical therapy, most virulent strains are resistant to antiviral drugs. Novel antiviral drugs or compounds are urgently needed to address this problem.

Isatis root is a kind of herbaceous plant widely cultivated and distributed in China. *Isatis* root is a joint therapeutic agent of influenza, fever, detoxification, and detumescence in Shennong herbal scripture [19,20]. In recent years, plant polysaccharides have been found to be energy resources that promote animal growth, and participate in animal immune regulation and have antitumor, antibacterial, antiviral, anti-inflammatory effects. *IRPS* has attracted much attention in the field of immunology and virology. Polysaccharides are one of the main components of *Isatis* root. As a macromolecule substance, it exhibits anti-oxidant, anti-inflammatory, and antiviral properties [21,22]. However, the antiviral effect of *IRPS* against PRRSV remains unclear. Previous studies have demonstrated that *IRPS* has substantial anti-oxidant and immunomodulatory activities in vitro, but few studies have been conducted in vivo [23,24]. Furthermore, gut microbes usually degrade polysaccharides through fermentation, producing metabolites including short-chain fatty acids, which participate in the metabolism and affect host physiological status [25–27]. Therefore, exploring the effect of polysaccharides on an organism is inseparable from the study of gut microbiota.

Recently, the development and application of “omics” technologies such as genomics, transcriptomics, proteomics, and microbiomics have provided new widely used experimental methods for understanding the molecular mechanisms driving biological processes, cell components, and molecular functions in cells and tissues [28–33]. In our study, we explored the antiviral effect of *IRPS* and investigated the expression changes of genes and proteins in three groups of piglets (mock group (M), prevention group (P) and infection group (I)) using transcriptome and proteome sequencing. Some key differentially expressed genes (DEGs), such as immune pathways, chemokine signaling pathways, and metabolic pathways, have highlighted the antiviral effects of *IRPS*. Furthermore, we evaluated the microbiomics in the above three groups of piglets. Our comparative analysis will help the better understanding of the antiviral effect of *IRPS* and develop novel antiviral therapies to provide a scientific reference for the prevention and treatment of PRRSV in the swine industry.

2. Results

2.1. Toxicity of *IRPS* on the Viability of Marc-145 Cells

The MTT assay confirmed that the concentration of *IRPS* used in subsequent experiments did not affect cell viability. The tested concentrations of *IRPS* were 0.447, 0.224, 0.112, 0.056, and 0.028 mg/mL. The results showed that *IRPS* had a cytotoxic effect when its concentration was higher than 0.224 mg/mL. Thus, *IRPS* concentrations of 0.027–0.112 mg/mL were selected for the next experiment.

2.2. Antiviral Effect of *IRPS* on NADC30-like PRRSV

The preventive and inhibitory effects of *IRPS* on PRRSV were investigated by MTT assays. When *IRPS* concentration increased from 3.5 to 112 µg/mL, it could prevent PRRSV infection.

To evaluate the effect of *IRPS* on PRRSV replication, Marc-145 cells were infected with 100 TCID₅₀ of PRRSV and were supplied with various concentrations of *IRPS*. The results showed that the inhibitory effect of *IRPS* on PRRSV replication was inconspicuous.

There was significant difference in OD570 between the 112 µg/mL of IRPS and 0 µg/mL of IRPS ($p < 0.05$) in inhibitory (Figure 1A) and direct groups ($p < 0.01$) (Figure 1C), respectively. When IRPS concentration increased from 56 to 112 µg/mL, the inhibition percentage increased in the inhibitory and direct groups (Figure 1D). In addition, we found that the IRPS prevented the PRRSV infection in a dose-dependent manner. We found significant differences in OD570 absorbance between 112 µg/mL and 0 µg/mL IRPS ($p < 0.0001$) (Figure 1B). The results showed that IRPS has clinical research potential to prevent PRRSV infection.

2.3. Clinical Signs and Histopathology

At 3 dpi, piglets in the infection group exhibited clinical signs of feed intake decreasing from 0.75 kg to 0.52 kg (per piglet). At 4 dpi, clinical signs improved in these piglets, such as messy fur, hypokinesia, anorexia, depression, and fever, and rectal temperatures increased by 0.2 °C to 0.5 °C. During the trial, group P and group M showed no clinical signs. The lungs were separated from the thoracic cavity and pathologically assessed by gross examination, H&E staining, and immunohistochemistry. The lungs exhibited serious hemorrhagic spots, congestion, and emphysema in group I. However, the typical lesions were slightly hemorrhagic spots on the surface of the lungs from group P piglets after being challenged with NADC30-like PRRSV strain, indicating the protective effect of IRPS on target organs.

To observe the histopathological changes in piglets, lung samples were fixed with formalin, embedded in paraffin, sectioned, and stained for further analysis. Analysis showed that the alveolar wall was seriously thickened in group I, and there was a small number of inflammatory cells in the pulmonary interstitium (Figure 1E). Some areas exhibited vascular smooth muscle cell necrosis, nucleolysis disappeared, and there was eosinophilic and homogenous in group P (Figure 1E). There was no significant pathological phenotype in the lungs of piglets in group M (Figure 1E). The results revealed that IRPS could significantly prevent and efficiently inhibit virus infection. Moreover, it exhibited a significant potential to improve the pathological injury of pig lung tissue.

2.4. Overview of Transcriptomic Analyses

In the transcriptomic analysis, 371 million clean reads and 95.93% clean reads were located on the *Sus scrofa* genome sequence. The Q30 base rate ranged from 92.84 to 93.45%, and 38.8–44.3 million clean reads were obtained per sample (Table S1). A total of 114,753 genes were detected in three groups by fragments per kilobase million (FPKM) mapped fragments. FPKM > 1 was used as the expression genes. A total of 1669 DEGs were identified in three groups using a cutoff of 2-fold change, FPKM > 1, and p -value < 0.05 [34]. There was a total of 1669 DEGs; 917 DEGs had higher expression levels and 752 DEGs displayed opposing tendencies. Among them, there were 870 (482 up-regulated and 388 down-regulated) in M vs. I (Figure 2A), 749 (417 up-regulated and 332 down-regulated) in P vs. I (Figure 2B), 50 (18 up-regulated and 32 down-regulated) in P vs. M (Figure 2C). More in group P and group M than group I, C-X-C motif chemokine ligand 10 (CXCL10), membrane-spanning 4-domains A7 (MS4A7), and interferon regulatory factor 7 (IRF7) had large values with $|\log_2 \text{fold changes}| > 2$. Meanwhile, group P and M were clustered together first and significantly separated from the group I (Figure 2D). The group M, group P, and group I samples shared 7 DEGs (Figure 2E).

As shown in Figure 2F, the expression trends for 20 genes in the three groups were consistent with the transcriptome analysis (Table S2). Meanwhile, qRT-PCR results showed that the transcriptome sequencing was reliable.

2.5. Gene Ontology Analysis and KEGG Pathway of DEGs

To further use DEG information, GO and KEGG analyses were used to identify relevant biological functions and pathways. As shown in Figure S1A, the mitotic cell cycle was the first place in M vs. I, defense response was the first place in P vs. I, and positive

regulation of long-term synaptic potentiation was the first place in P vs. M in the biological process (BP). In molecular function (MF), carbohydrate derivative binding accounted for the largest proportion in M vs. I, chemokine activity occupied the largest proportion in P vs. I, and active transmembrane transporter activity occupied the largest proportion in P vs. M. In cellular components (CC), the chromosome and centromeric region were the largest category in M vs. I, the extracellular region was the largest category in P vs. I, and basement membrane was the largest category in P vs. M.

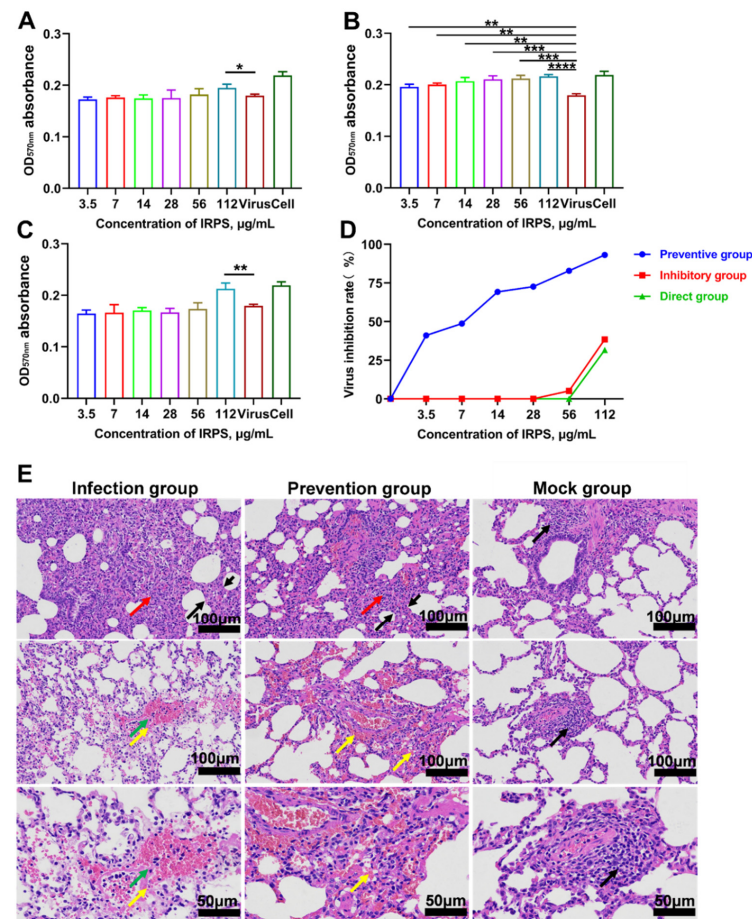


Figure 1. Antiviral study of *IRPS* in vivo and in vitro. (A) Inhibitory effect of *IRPS* on PRRSV; in the inhibitory assay, at 1.5 h PRRSV infection, cells were treated with different concentrations of *IRPS* and cell status was observed; (B) Preventive effect of *IRPS* on PRRSV; in the preventive assay, cells were treated with different concentrations of *IRPS* for 4 h, then 1.5 h PRRSV infection to observe cell status; (C) The direct effect of *IRPS* on PRRSV; in the direct assay, PRRSV was mixed with various concentrations of *IRPS* and incubated for 1.5 h to observe cell status; (D) Percentage inhibition of *IRPS* on PRRSV; Virus: the concentration of *IRPS* was 0 µg/mL. Cell: the normal growing cell. * ($p < 0.05$), ** ($p < 0.01$), *** ($p < 0.001$), **** ($p < 0.0001$). (E) Effect of *IRPS* on lung histopathology of PRRSV-infected piglets. Histological observation of representative lungs from three groups (H&E stain, 100× and 50× magnification). Infection group: severe thickening of alveolar walls in local tissue (black arrow); alveolar cells can be observed in a small inflammatory cell infiltration (red arrow). local vascular smooth muscle cell necrosis, nuclear dissolution disappears, and eosinophilic homogeneous (yellow arrow); surrounding bleeding (green arrow). Prevention group: local alveolar wall thickening of tissue (black arrow); alveolar wall can be seen in a small inflammatory cell infiltration (red arrow); local hemorrhage, alveolar cavity, and blood vessels can be seen with more red blood cells (yellow arrow). Normal control group: lung tissue of blank group. Tissue alveolar; the bronchial structure is clear; thin alveolar wall; and small inflammatory cell infiltration (black arrow) around bronchial and blood vessels (black arrow); the branch structure is complete, and the epithelial cell morphology is normal.

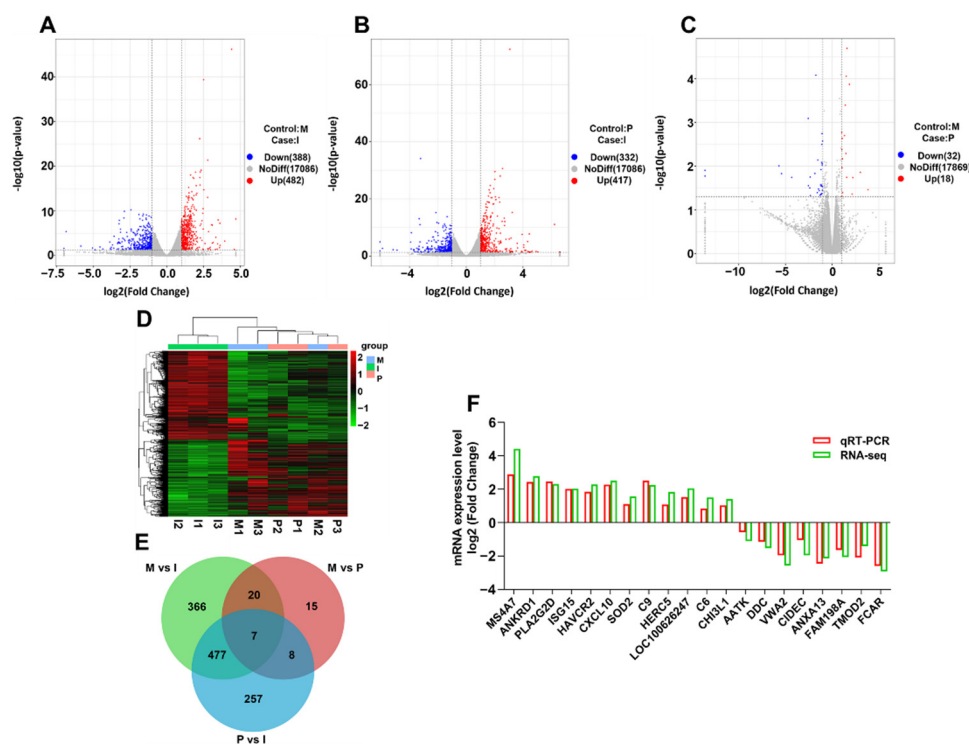


Figure 2. Transcriptome differences between the piglet lung tissue samples. Plot showing the \log_2 fold change and the $-\log_{10}(p\text{-value})$. The red points represented the up-regulated DEGs, and the green points represented the down-regulated DEGs ($|\log_2 \text{fold change}| > 1$, $p\text{-value} < 0.05$). (A) group P vs. group I; (B) group M vs. group I; (C): group M vs. group P; (D) Heat map of the DEGs in different groups; (E) using the Venn diagram for standard or unique DEGs; (F) qRT-PCR analysis of 20 DEG expression changes. The levels of β -actin normalized relative mRNA expression levels.

We compared these DEGs to investigate the known immune and signaling pathways to identify the related biological functions and pathways. There were 101 KEGG pathways differentially expressed in the P vs. M samples, 261 KEGG in the P vs. I, and 261 KEGG in the M vs. I, respectively. As shown in Figure S1B, the top 20 KEGG pathways were screened based on the number of DEGs. Three pairwise comparisons (M vs. I, P vs. I, and P vs. M) involved cell growth and death, the immune system, signaling molecules, and interaction pathways. The specific metabolic pathways are as follows: cytokine–cytokine receptor interaction, cell cycle, DNA replication, and chemokine signaling pathway, toll-like/NOD-like receptor-signaling pathway, cell adhesion molecules (CAMs), and long-term potentiation.

2.6. Proteomic Analysis and Identification of Differentially Expressed Proteins

There were 39,045 identified peptide-spectrum matches (PSM) that matched 18,343 peptides and 4398 protein groups. The EDPs were screened between P and I, between M and I, and between P and M was performed by proteomics. Using a threshold of 1.5-fold change and $p < 0.05$ to define DEPs, a total 370 DEPs (195 up-regulated and 175 down-regulated) were detected in the three group samples. Among these DEPs, there were 89 DEPs (38 up-regulated and 51 down-regulated) in the P vs. I, 135 DEPs (64 up-regulated and 71 down-regulated) in the M vs. I, and 146 DEPs (93 up-regulated and 53 down-regulated) in the P vs. M (Figure S2).

As shown in Figure 3A, in BP, the immune-system process was first place in M vs. I, the multi-organism process was first place in P vs. I, and cellular component organization or biogenesis was first place in P vs. M. In MF, chemorepellent activity accounted for the largest proportion in M vs. I, binding occupied the largest proportion in P vs. I, and molecular function regulator occupied the largest proportion in P vs. M. In CC, the

chromosome and centromeric region was the foremost category in M vs. I, binding was the foremost category in P vs. I, and supramolecular fiber was the foremost category in P vs. M.

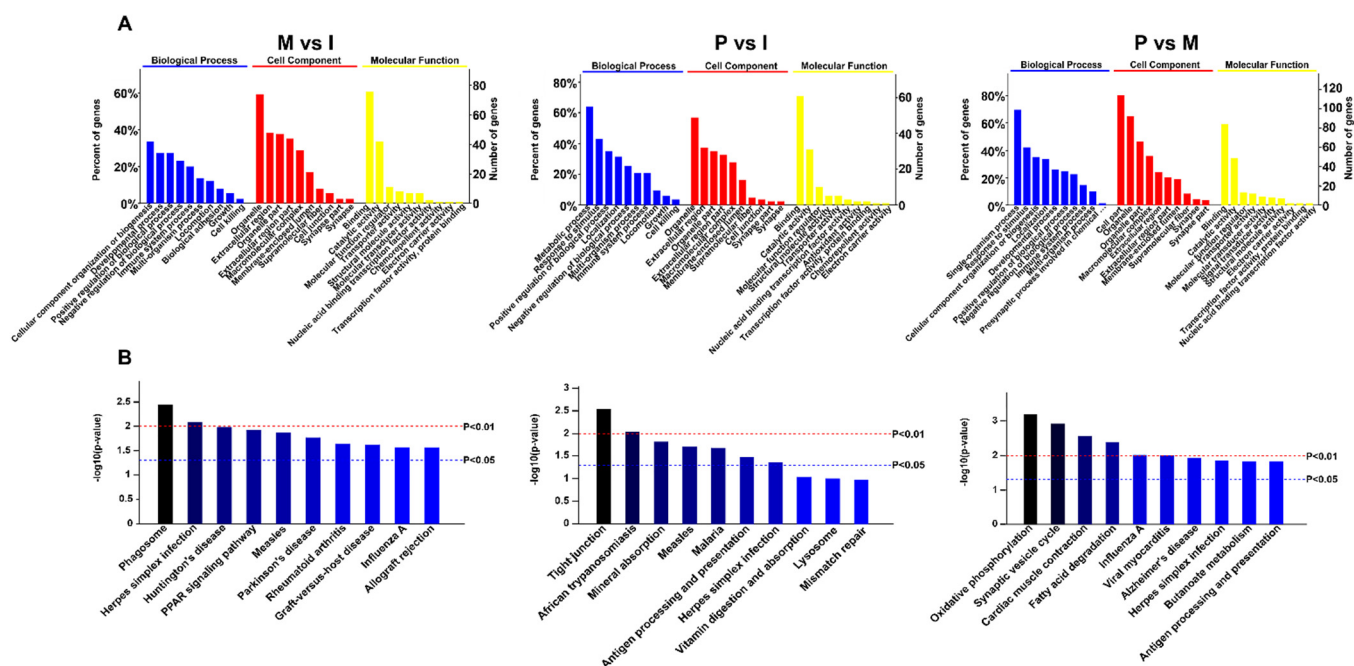


Figure 3. Identification and function analysis of DEPs. (A) GO analysis of the DEPs; (B) KEGG analysis of the DEPs.

KEGG functional enrichment analysis of the DEPs revealed that primary immune-related pathways, such as herpes simplex infection and measles, were enriched in M vs. I and P vs. I, antigen processing and presentation was enriched in M vs. I and P vs. M, and influenza A was enriched in M vs. I and P vs. M. It is noteworthy that the PPAR signaling pathway and rheumatoid arthritis were enriched in M vs. I, tight junction and mineral absorption were enriched in P vs. I, and oxidative phosphorylation, fatty acid degradation, and butanoate metabolism were enriched in P vs. M (Figure 3B).

2.7. Correlation Analysis of DEGs and DEPs

In M vs. I, P vs. I, and P vs. M, the R values of the correlation coefficient were 0.387, 0.412, and 0.055 between proteome and transcriptome (Figure 4A–C). To correlate transcript and protein expression profiles, accession numbers were extracted from the proteome and compared with annotated RNA-Seq libraries, which found 33 proteins corresponding to DEPs and DEGs (Table S3). A total of 30 of the 174 proteins had the same expression levels as mRNA levels, including 19 proteins from M vs. I, and 11 proteins from P vs. I. The 33 DEGs and DEPs were conducted by cluster analyses (Figure 4D). Then, 30 genes showed similar regulation, and 3 genes showed opposite regulation, after comparison at transcript and protein levels.

2.8. Effects of IRPS on Gut Microbiota Diversity

2.8.1. The Microbial Community Diversity of Piglets

In this study, the number of effective sequences in each sample exceeded 75,000. The length distribution of piglet samples was about 400–450 bp. Figure 4 shows the ASVs of each piglet at Phylum, Class, Order, Family, Genus, and Species levels. Over 220 ASVs have been identified per sample at the Species level (Figure 5A). The Venn diagram reveals 710 bacterial species in all three groups. Interestingly, there were 282 bacterial species in group I and group P, but not found in group M (Figure 5B).

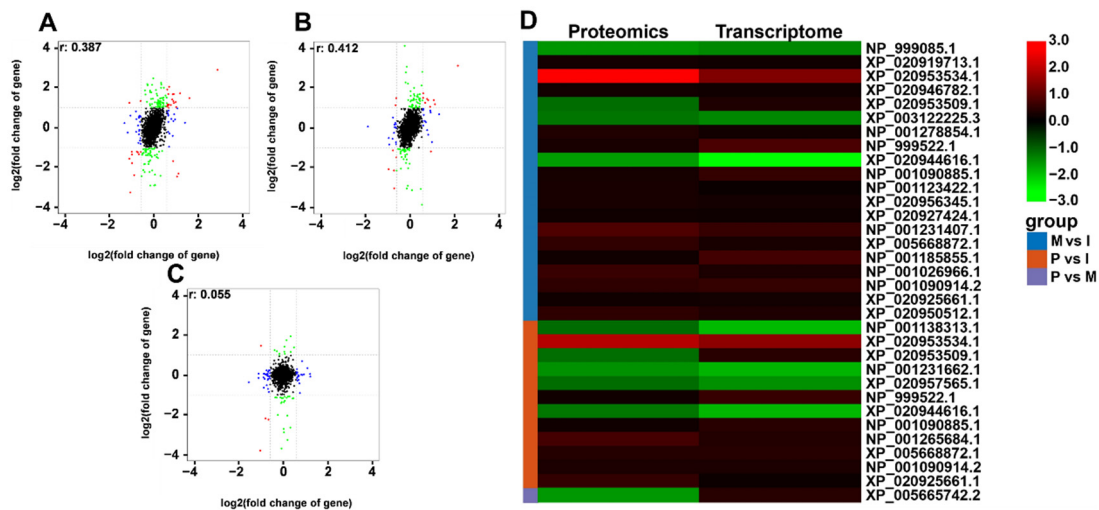


Figure 4. Correlation analysis of proteomics and transcriptome. (A–C) The correlation analysis of proteomics and transcriptome in M vs. I, P vs. I, P vs. M. In related analysis diagram, DEGs level for absolute fold change ($|\log_2 \text{fold change}| = 1$), and the DEPs was absolute fold change ($|\log_2 \text{fold change}| = 0.585$) as thresholds for Pearson correlation analysis. Red indicates that the transcript and protein levels are significantly differentially expressed. Blue indicates that the protein levels are significantly differentially expressed. Green indicates that the transcript levels are significantly differentially expressed. Black indicates that the transcript and protein levels are not significantly differentially expressed; (D) The expression pattern clustering analysis for 33 DEGs and DEPs with correlations. Red indicates up-regulated, and green indicates down-regulated.

2.8.2. Alpha Diversity and Beta Diversity

In this study, seven indices were used to represent community diversity. There were no significant changes among groups M, P, and I ($p > 0.05$) (Figure 5C). Principal coordinate analysis (PCoA) can reflect the similarity between samples according to the projected distance of samples on the coordinate axis [35]. Using weighted UniFrac distance-based PCoA, Figure 5D showed that the projection distance of group I was the farthest from group M and P, while group P was the closest to group M, indicating that *IRPS* had an improved effect on the microbiota composition of infected piglets.

2.8.3. Gut Microbiota Community Structure Analysis

At the Phylum level, firmicutes (74.27% in group P, 51.18% in group I, 68.72% in group M), bacteroidetes (17.75% in group P, 41.46% in group I, 17.64% in group M), and spirochaetes (5.19% in group P, 4.14% in group I, 10.93% in group M) were found to be the major microbial community of all piglets (Figure S3A). At the Genus level, streptococcus was found to be much higher in group M (35.1%) and group P (29.95%) than group I (0.27%), while prevotella was found to be much higher in group I (27.63%) than group P (6.33%) and group M (7.15%). Treponema was found to be much higher in group M (10.52%) than group P (4.96%) and group I (3.86%). There was no visible difference among different groups of oscillopsia. Roseburia was found to be much higher in group I (8.9%) than group P (0.09%) and group M (0.1%) (Figure S3B).

2.8.4. Comparison of the Microbial Community Structure among Different Piglet Groups

At the Phylum level, the dominant bacteria were composed of firmicutes, bacteroidetes, and spirochaetes in each group. Among them, firmicutes abundance was highest in the three groups, and *IRPS* had a significant effect on it ($p < 0.05$). Compared to group I, group P was characterized by higher firmicutes levels. The relative abundance of bacteroidetes in groups P and M was significantly lower than group I ($p < 0.05$) (Figure 6A). At the Genus level, compared to the group I, streptococcus, roseburia, and phascolarctobacterium

were significantly different, with $p < 0.05$ and prevotella ($p < 0.01$) in group P. However, compared to group I, streptococcus and roseburia were significantly different at $p < 0.05$, while prevotella, SMB53, and phascolarctobacterium were extremely significant different at $p < 0.01$ in group M (Figure 6C). Meanwhile, we found a difference in gemmiger and anaerovibrio between group I and other groups using heat map analysis (Figure 6B).

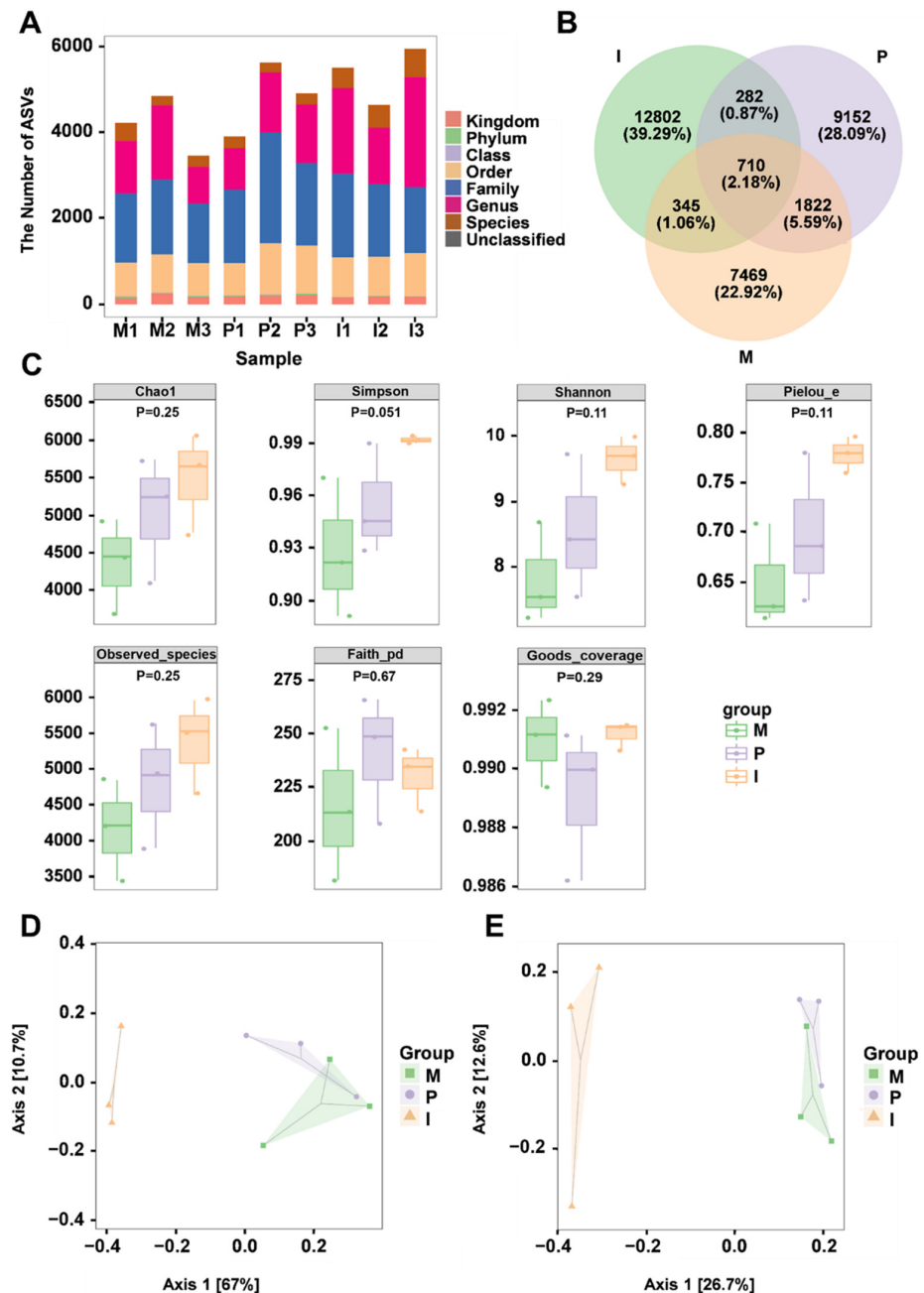


Figure 5. IRPS modulated the composition of gut microbiota. (A) The quantity of ASVs in different piglet samples; (B) Venn diagram of comparison of ASV distribution in different groups; (C) Comparison of the microflora microbial diversity index (Chao1, Simpson, Shannon, Pielou's evenness, Observed species, Faith's PD) between piglet groups; (D) weighted UniFrac distance-based PCoA; (E) unweighted UniFrac distance-based PCoA. Axis 1 (X) and 2 (Y) represent the main axes of objects changing in two-dimensional space. Each point in the graph represents a sample, and the dots of different colors indicate different groups of samples. The closer the projection distance of the two points on the coordinate axis, the more similar the community composition of the two samples in the corresponding dimensions.

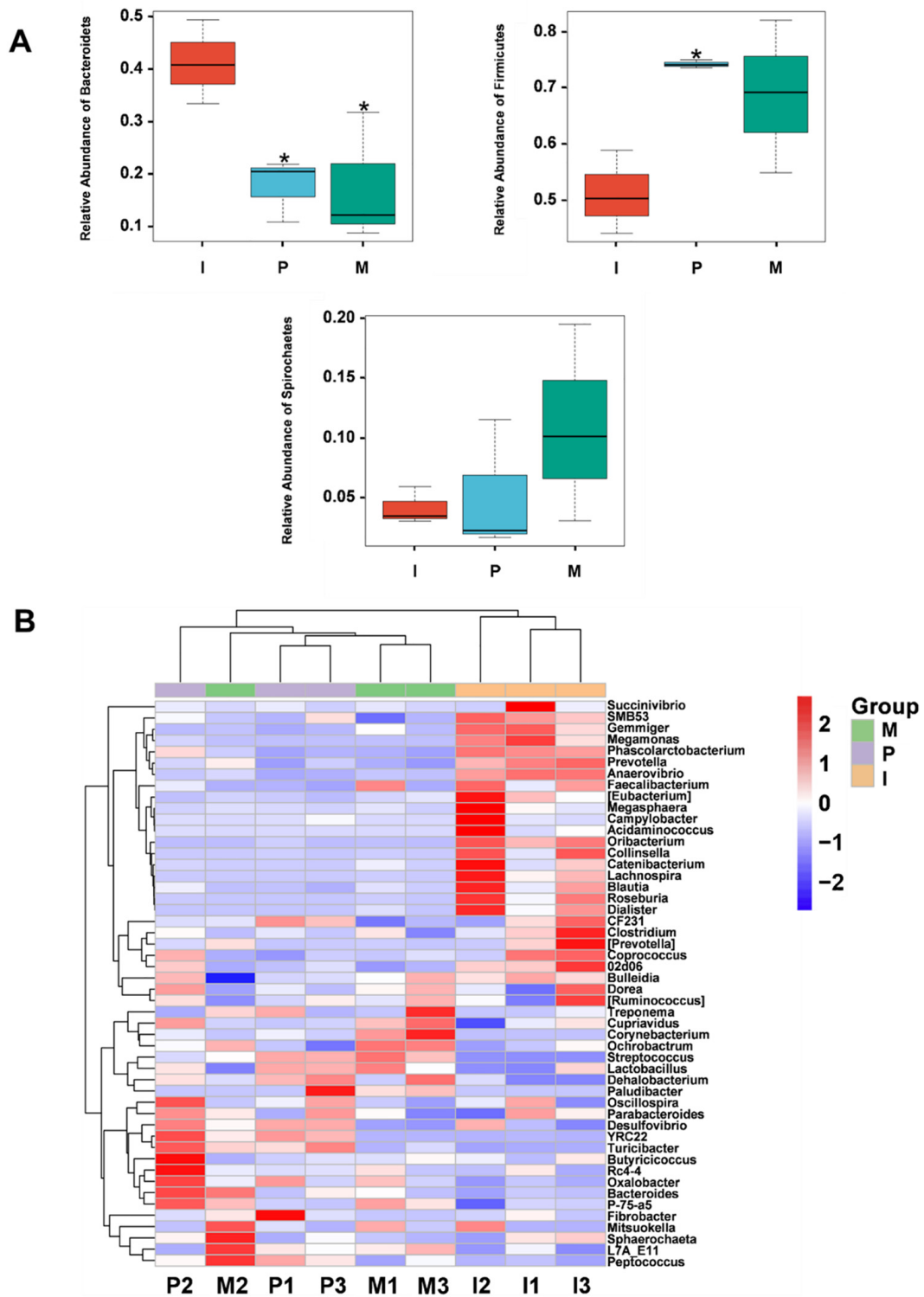


Figure 6. Cont.

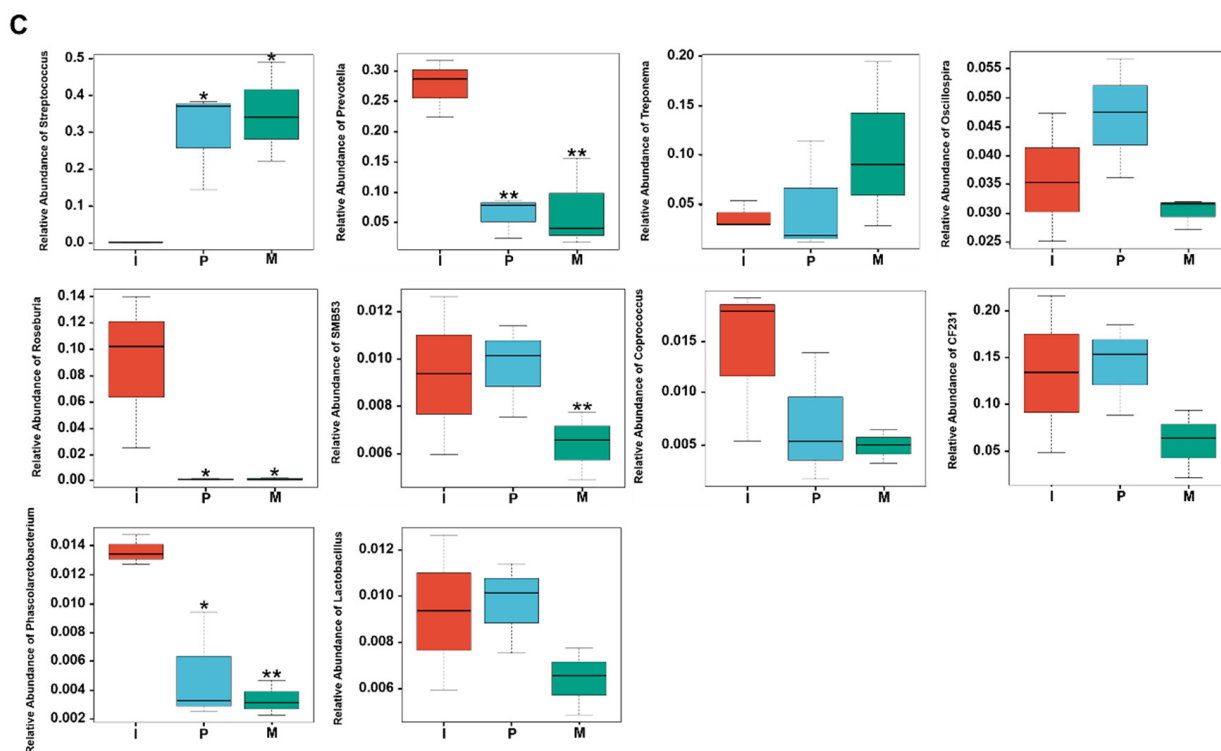


Figure 6. Comparative analysis of gut microbial community structure in different piglet groups. (A) Comparison box chart of microbial community structure at the Phylum level; red represents group I, blue represents group P, green represents group M; (B) Heat map of the 50 most abundant genera of each group; the red block indicates that the Genus was more abundant in that sample than in other samples, and the blue block indicates that the Genus was less abundant in that sample than in other samples; (C) Comparison box chart of microbial community structure at the Genus level. Different asterisks indicate significant differences * ($p < 0.05$), ** ($p < 0.01$).

3. Discussion

In this study, *IRPS* was proved to prevent and efficiently inhibit virus infection in vitro and in vivo. In addition, the objective was to explore the potential immune mechanism of *IRPS* involvement in the antiviral response of piglets. There were analyses that identified many DEGs and DEPs using transcriptome and proteome sequencing. In addition, the changes in intestinal flora were observed by 16S sequencing.

Isatis root, a traditional Chinese medicine (TCM) known for its widely antiviral effects, has a medical history of thousands of years in China and other Asian countries [21]. It has been reported that *IRPS* has antiviral effects on swine influenza virus (SIV), herpes simplex virus 1 (HSV-1), pseudorabies virus (PRV), and severe acute respiratory syndrome (SARS). We compared and integrated the antiviral effects of *IRPS* in vitro (preventive effect, inhibitory effect, and direct effect). The results showed that *IRPS* has a preventive effect. Subsequently, the preventive effect of *IRPS* was demonstrated in vivo. Interestingly, it exhibited significant potential to improve the pathological injury of pig lung tissue.

In this investigation, the DEGs and DEPs of SLA-2, CD180, ANXA13, MX2, CD14, LOC110261034, and DHX58 were found in group I and group P (as also observed in the study by Lim [34]). Furthermore, DDX58, DCN, CD163, AK1, PCNA, KIF23, CTSB, OAS2, and GZMA were found in group I, but not in other groups (Table S3). DDX58, OAS2, and CXCL10 were highly expressed in 3 dpi. OAS2 is one of the 2–5A synthetase families, which promote the degradation of viral RNA and the inhibition of viral replication [36]. CD163 is a receptor required for PRRSV infection and its expression is regulated by a variety of inflammatory mediators. Several studies have shown that CD163 is an essential receptor involved in the uncoating of virions, blocking or down-regulating CD163 expression to

restrict PRRSV infection [37–40]. In our study, there was no significant change in mRNA and protein levels of CD163 between P and I, suggesting that CD163 was more likely to be related to an *IRPS* antiviral effect. Moreover, *IRPS* may reduce PRRSV infection by inhibiting or blocking the expression of CD163.

PRRSV may be similar to other RNA viruses or coronaviruses. Coronavirus is a single-stranded RNA virus. PRRSV produces dsRNA early during the infection cycle due to genome replication and mRNA transcription [41,42]. The DEGs/DEPs could be mapped to the immune pathways of piglets. Among them, the DEGs/DEPs were mapped onto the NOD-like receptor-signaling pathway using the KEGG database. Oligoadenylate synthetase (OAS), NLR Family Pyrin Domain Containing 3 (NLRP3), Caspase 1 (CASP1), and Interleukin 18 (IL-18) were significantly up-regulated in group I vs. group M. Interleukin-1 beta (IL-1 β) showed no significant changes. Previous studies have shown that the non-structural protein 11 of PRRSV inhibits NLRP3 inflammasome-mediated induction of IL-1 β [43]. On the other hand, PRRSV could induce early IL-1 β expression and secretion in porcine alveolar macrophages (PAMs) via the NLRP3 inflammasome pathway. However, the levels of pro-IL-1 β mRNA and IL-1 β protein decreased to a certain extent after infection [44].

NLRP3 only changed in group I, and no significant change was found in other groups. The *IRPS* was secure for the host and non-activate inflammatory pathways. NLRP3 inflammasome induces maturity and secretion of proinflammatory IL-1 β and IL-18 as a multiprotein complex. The maturation of IL-1 and IL-18 leads to signaling cascades that regulate the expression of tumor necrosis factor alpha (TNF- α), interferon gamma (IFN- γ), and other cytokines; these recruit the lymphocytes, linking innate and adaptive immune responses to control the invading pathogens [45–47].

In the past decade, numerous studies have attributed to the prevotella species. They have been abundant under inflammatory conditions, such as rheumatoid arthritis (RA), periodontitis, intestinal dysbiosis, and inflammation in HIV patients. The previous report indicated that increased prevotella in human immunodeficiency virus (HIV) is a driver of persistent gut inflammation, leading to mucosal dysfunction and systemic inflammation [48–50]. *IRPS* could inhibit prevotella and reduce inflammatory response in our study. Furthermore, the relative abundance of streptococcus also returned to normal levels.

These results suggest that *IRPS* not only inhibits inflammatory gene expression, but also reduces the inflammatory response of hosts. In a previous study, astragalus polysaccharide (APS) was found to alleviate colitis in mice by inhibiting NLRP3 inflammasome [51]. Thus, the inhibitory effect of *IRPS* on PRRSV-induced inflammation may be due to the inhibition of the NLRP3 gene expression, and affect the expression of downstream genes. The antiviral mechanism of *IRPS* against PRRSV is summarized in Figure 7. In summary, we report here provide a molecular rationale to explain the broad antiviral properties of *IRPS*.

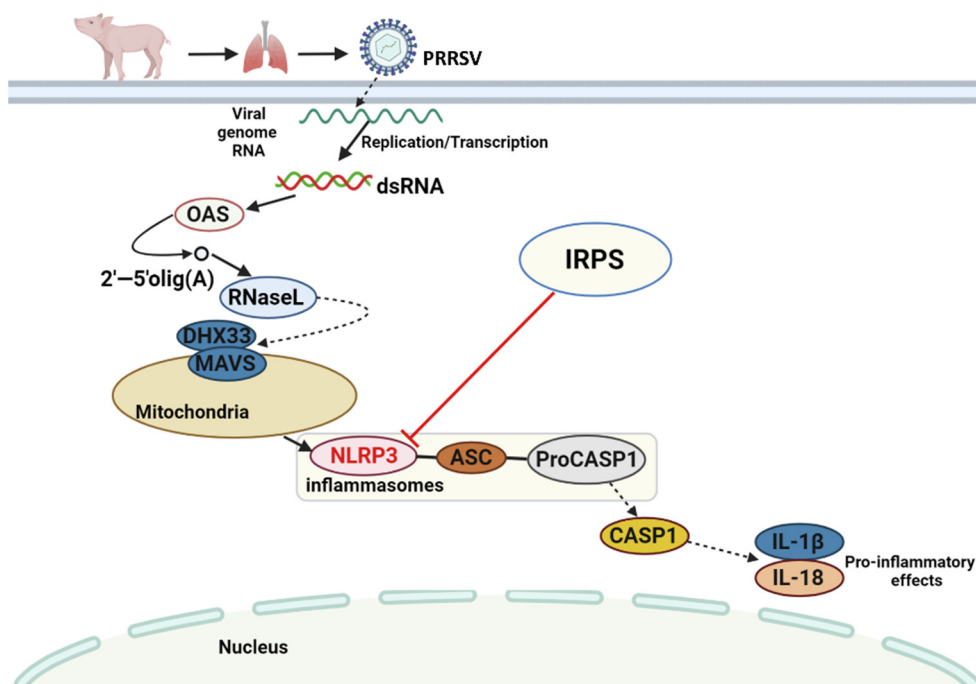


Figure 7. Schematic presentation of the *IRPS* anti-PRRSV molecular mechanism. The graphic was created with BioRender.com. PRRSV becomes double-stranded RNA (dsRNA) by replication and transcription, and acts directly on OAS gene. OAS gene could promote RNaseL expression. RNaseL acts indirectly on DHX33 and MAVS, which in turn activate inflammasomes (NLRP3, ASC, ProCASP1). Then, the inflammasomes act indirectly on CASP1, and finally activates IL-1 and IL-18, thus triggering inflammation in the body. -----▶ activation; —▶ expression; —▶○▶ indirect effect; —| inhibitory effect.

4. Materials and Methods

4.1. Preparation of *IRPS*

Isatis root was purchased from Beijing Shengtaier Biological Technology Co., Ltd. (Beijing, China). The preparation of *IRPS* from *Isatis* root was performed by the phenol-sulfuric acid method. Briefly, *Isatis* root crude extracts were immersed in deionization water for dissolution. Subsequently, 1 mL solution was mixed with 1.0 mL of 6% phenol solution. After being mixed well, 5.0 mL of concentrated sulfuric acid was added and mixed immediately. The solvent was heated at 70 °C for 20 min and stored at 16 °C. The absorbance values of OD570 were measured using an automated plate reader (Bio-Rad, Hercules, CA, USA). All samples were prepared in triplicate. The final concentration of *Isatis* root polysaccharide was 0.447 mg/mL.

4.2. Virus and Cells

NADC30-like PRRSV strain used in this study was isolated from a farmed pig in Sichuan province, China, in 2016. In short, the representative clinical symptoms include persistent high fever, anorexia, blue ears, and conjunctivitis. Clinical specimens (lung, liver, lymph) were collected for detection, and the virus was identified as the NADC30-like PRRSV strain by PCR and sequencing techniques. In the previous experiments, 50% tissue culture infection dose (TCID₅₀) of the 10^{4.36}·100 μL⁻¹ was calculated by the Reed–Muench method.

Monkey kidney (Marc-145) cell line was maintained at the college of veterinary medicine (Sichuan Agricultural University, China). According to the standard culturing procedure, cells were cultured with DMEM containing 10% fetal bovine serum, 100 U/mL penicillin, and 100 U/mL streptomycin at 37 °C with 5% CO₂.

4.3. Animal Protocol and Statement

Fifteen male piglets (three-breed cross; 5–6 weeks old; 10–13 kg) were purchased from Chengdu Wangjiang agriculture and animal husbandry technology Co., Ltd. (Chengdu, China). According to qPCR diagnosis, all piglets have not been vaccinated or infected with common porcine pathogens. All animal experiments were approved by the institutional animal care and use committee of Sichuan Agricultural University of China (Approval number SYXK2019-187). All animal experiments were performed under Laboratory Animals Welfare and Ethics published by the General Administration of Quality Supervision, Inspection and Quarantine of the People's Republic of China. All animals were individually housed under controlled temperature (26 °C), humidity (60%), and lighting (12 h/day), with free access to water.

4.4. Anti-NADC30-like PRRSV Activity In Vitro

4.4.1. Determination of IRPS Cytotoxicity

The methyl thiazolyl tetrazolium (MTT) assay was used to evaluate the cytotoxicity effect of IRPS in Marc-145 cells [23,52]. Marc-145 cells were inoculated into 96-well culture plates with 2.4×10^4 cells/well. After 36 h of culture, different concentrations of IRPS were added to each well and maintained for 120 h in triplicate. Then, MTT reagent was supplied and incubated at 37 °C with 5% CO₂ for 4 h followed by adding 100 µL of DMSO (Gibco, Grand Island, NY, USA) in each well. The optical densities (OD) values were measured at the wavelength of 570 nm using an automated plate reader (Bio-Rad, Hercules, CA, USA).

4.4.2. Determination of IRPS Cytotoxicity

The MTT assay was used to evaluate the preventive effect of IRPS on PRRSV replication [53]. Marc-145 cells were cultured for 24 h and reached at least 80% confluence in 96-well plates. Then, the culture medium was refreshed in each well with various concentrations of IRPS. After incubation for 4 h, IRPS was washed with PBS three times for removal, and the cells were infected with PRRSV of 100 TCID₅₀ for 1.5 h. Subsequently, the non-absorbed viral particles were discarded by being washed with PBS three times and supplied with fresh culture medium. The cells were then incubated at 37 °C with 5% CO₂. The control group cells (non-added IRPS) were incubated to reach at least 80% cytotoxicity. The infection percentage of PRRSV was determined by the following formula: virus inhibition rate (%) = $(OD_t - OD_v)/(OD_c - OD_v) \times 100$, in which the OD_t, OD_c, and OD_v represent the absorbance of tested substances (cells, virus, IRPS), cell control (cells) and virus control (cells, virus) [24].

Marc-145 cells were cultured in 96-well plates, as described. When the cell culture reached at least 80% confluence for 24 h, the medium was removed, and 100 TCID₅₀ of PRRSV was added to each well. After incubation for 1.5 h, the virus was washed with PBS three times to remove the unabsorbed virus. Then, the various concentrations of IRPS were added to each well. The MTT assay was used to evaluate the inhibitory effect of IRPS as previously mentioned.

Briefly, several different concentrations of IRPS were thoroughly mixed with PRRSV of 100 TCID₅₀ and incubated at 37 °C for 1 h. Then, the mixture was added to cells with at least 80% confluence. After incubation for 1.5 h to observe cell status, the MTT assay was used to evaluate the direct effect of IRPS on PRRSV by the above method.

Statistical analysis was performed with GraphPad Prism 8.0.2 (GraphPad Software, San Diego, CA, USA) using the *t*-test.

4.4.3. Antiviral Effect of IRPS In Vivo

After 7 d of domestication, 15 piglets were randomly divided into three groups (n = 5). Group 1 was the infection group. Group 2 was the prevention group. Group 3 was the mock group. Group 2 was treated by feeding with doses of *Isatis* root granule (0.1 g/kg/d).

After 15 days of feeding, all piglets were slightly anesthetized and intranasally inoculated with 105.38 TCID₅₀ of NADC30-like PRRSV, except group 3, who were inoculated

with culture medium. Then, oral and nasal samples were collected at 5 days post-challenge for the detection of the PRRSV NADV30-like genomic RNA by qPCR. All piglets were observed to record clinical signs, such as mental state, breathing, and eating habits. Any piglet deaths were recorded during the PRRSV challenge, and they were euthanized on day 15. In addition, lung tissue samples were collected and fixed in 4% buffer formaldehyde solution for 1 d. They were embedded in paraffin, sectioned, and stained with eosin. Subsequently, the slides were observed under a microscope.

4.5. RNA Extraction and Sequencing

The lung tissue samples were collected from three groups of piglets (group I: infection group; group P: prevention group; group M: mock group.). Total RNA was extracted from lung tissues using the TRIzol reagent according to the manufacturer's protocol. The concentration and quality of RNA were evaluated by NanoDrop 2000 Spectrophotometer and Agilent 2100 Bioanalyzer. The cDNA libraries were constructed using only high-quality RNA (RNA integrity number, RIN > 7.0). All libraries were sequenced on a HiSeq 4000 with paired end (PE, 350 bp). By removing reads containing adapters, low-quality reads, and reads containing more than 5% N (default parameters), the obtained raw data were filtered into clean data with FASTP, and then mapped to the pig reference genome of *Sus scrofa* 11.1 using HISAT2 [54,55]. The gene expression levels of fragments per kilobase million (FPKM) were analyzed. Absolute fold change ($|\log_2 \text{fold change}| > 1$) and p -value < 0.05 were used as the thresholds for screening DEGs [56]. We used R-package ClusterProfiler for Gene Ontology (GO) enrichment to analysis DEGs. The statistical enrichment of DEGs analysis was conducted using R software according to the Kyoto Encyclopedia of Genes and Genomes (KEGG) pathways [32,57,58].

4.6. Quantitative Real-Time PCR Validation

Total RNA was extracted from the lung tissue of nine piglets (group I, group P, group M) for qRT-PCR analysis. The expressions of 20 swine-related genes (12 up-regulated and 8 down-regulated) were verified by quantitative real-time PCR (qRT-PCR). All experiments were carried out 3 times. The expression levels of internal reference gene were normalized to β -Actin levels. The qRT-PCR reaction was conducted as follows: 95 °C for 3 min, a total of 40 cycles of 95 °C 10 s, 59 °C 10 s, and 72 °C 30 s. The relative gene expression levels were evaluated by $2^{-\Delta\Delta C_t}$ method [59].

4.7. Tandem Mass Tag-Based on Proteomics

Differentially expressed proteins (DEPs) were detected in the piglets with divergent lung traits by isobaric tandem mass tags (TMTs). Each peptide was about 80 μg . The total protein (100 μg) was removed from each sample solution and digested with trypsin (Thermo Fisher Scientific, Waltham, CA, USA) at 37 °C for 16 h at a protein:trypsin ratio of 30:1. After digestion, the peptides were dried by vacuum centrifugation. TMT labeling was performed on ten-plex kit (Thermo Fisher Scientific, San Jose, CA, USA) according to the manufacturer's instructions. Nine samples (3 biological replicates from the Mock group, 3 biological replicates from the infection group, 3 biological replicates from the prevention group) were TMT labeled: 126-, 127C-, and 128N-TMT tags for the control group; 128C-, 129N-, and 129C-TMT tags for infection group; 130N-, 130C-, and 131- for the prevention group. Then, the labeled samples were analyzed using liquid chromatography-tandem mass spectrometry (LC-MS/MS) [60]. Based on a previous study, the Easy-nLCTM 1200 ultra-high-performance liquid chromatography (UHPLC) system (Thermo Fisher Scientific, Waltham, MA, USA) was used for strong cation exchange (SCX) chromatography [61]. The peptide was analyzed by Q-Exactive mass spectrometer, positive ion mode, and the selected mass range was 300–1800 mass/charge (m/z).

The raw files were first merged and converted into an MGF file by Proteome Discoverer 1.4 (Thermo Fisher Scientific, San Jose, CA, USA). Then, a search was performed on the Uniprot database of swine (*Sus scrofa*) Mascot 2.2 search engine (Matrix Science,

London, UK) with 180,744 entries. The relevant parameters are as follows (Table 1). Protein expression levels with a cutoff of 1.5-fold change and p -value < 0.05 were determined as significant DEPs. For bioinformatics analysis, the parameter sets were the same as those in the study of Wang et al. [31].

Table 1. Protein samples retrieved; qualitative and quantitative parameters.

Item	Value
Type of search	MS/MS Ion search
Enzyme	Trypsin
Mass Values	Monoisotopic
Max Missed Cleavages	2
Fixed modifications	Cabamidomethyl (C), TMT 10 plex (N-term), TMT 10 plex (K)
Variable modifications	Oxidation (M), TMT 10 plex (Y)
Peptide Mass Tolerance	±20 ppm
Fragment Mass Tolerance	0.1 Da
Protein Mass	Unrestricted
Database	uniprot_Sus_scrofa_180744_20200117.fasta
FDR	≤0.01
Protein Quantification	Use only unique peptides
Experimental Bias	Normalize on protein median

Using QuickGO (<http://www.ebi.ac.uk/QuickGO/>) (accessed on 21 June 2021) Fisher's exact test evaluated the significance level of the GO term after DEP enrichment, and considered p -value < 0.05 as significant. According to the Kyoto Encyclopedia of Genes and Genomes (KEGG) pathway database (<https://www.kegg.jp/kegg>) (accessed on 27 June 2021), metabolic pathway analysis was conducted using R software, version 3.5.1 (used on 2 August 2021).

4.8. DNA Extraction of Intestinal Contents and Sequencing

Fresh feces samples were collected from the infection group ($n = 3$; marked as I1, I2, I3), prevention group ($n = 3$; marked as P1, P2, P3), mock group ($n = 3$; marked as M1, M2, M3). According to the manufacturer's directions, total microbial genomic DNA was extracted from three groups of samples using the QIAam DNA Mini Kit (Qiagen, Hilden, Germany). The PCR was amplified the V3–V4 region of 16S rRNA genes and sequenced on the Illumina MiSeq/NovaSeq platform.

The incorrect or error sequences were removed by Quantitative Insights into Microbial Ecology, v.2019 (QIIME2) [62]. QIIME2 employs the Divisive Amplicon Denoising Algorithm (DADA2) to identify amplicon sequence variants (ASVs). DADA2 is an open-source software package for modeling and correcting amplicon errors in Illumina sequencing. DADA2 accurately infers sample sequences without coarse graining into OTUs, and resolves only one nucleotide [63,64]. Then, ASVs were taxonomically grouped and classified by plotting classify-sklearn (<https://github.com/QIIME2/q2-feature-classifier>) (accessed on 14 July 2021) against a curated Greengenes database (Release 13.8, <http://greengenes.secondgenome.com/>) (accessed on 20 July 2021) [65,66]. Seven indices of alpha diversity were computed (Chao1 and Observed species, Faith's PD, Simpson and Shannon, Pielou's evenness, Good's coverage) [67–73]. Principal component analysis was used to analyze the beta diversity of microbial community structure similarity [74]. QIIME2 was used for statistics of microbial community structure in Phylum, Class, Order, Family, Genus, and Species of each group.

For statistical analysis, the parameters were set the same as in the study by Chen et al. [27]. All data were analyzed by one-way ANOVA, followed by multiple comparisons using the Tukey test.

5. Conclusions

In conclusion, this study was the first attempt to investigate the complexity of *IRPS* antiviral effects against PRRSV at the transcriptome and proteome levels of piglets. The interpretation of two omics data revealed many candidate genes and proteins that may be involved in the antiviral effect of *IRPS* against PRRSV mechanisms of the piglet. These DEGs or DEPs were involved in the immune-system and infectious-disease (viral) pathways, such as toll-like and Nod-like receptor-signaling pathway, Influenza A, herpes simplex infection, and chemokine signaling pathway. Further studies demonstrated that the antiviral effect of *IRPS* might be related to the Nod-like signaling pathway, which mainly reduces the inflammatory response by inhibiting the NLRP3 caspase-1 gene expression. Our findings will facilitate further research aimed at identifying essential genes and proteins active during the antiviral activity of *IRPS* against PRRSV. However, more work is needed to clarify the specific functions of these identified genes and proteins. Furthermore, this study demonstrated that *IRPS* might impact PRRSV infection in piglets by intervention or modulation of gut microbiota. Moreover, *IRPS* could restore the microbial community richness of infected piglets and has a potentially beneficial effect on the host by mediating the structure of gut microbiota.

Supplementary Materials: The following supporting information can be downloaded at: <https://www.mdpi.com/article/10.3390/ijms23073688/s1>.

Author Contributions: Methodology, D.J., X.W.(Xulong Wu), X.W.(Xinping Wang) and Y.W.; software, P.Z.; validation, D.J., G.Z. and L.Z.; formal analysis, G.Z.; investigation, G.Z. and L.Z.; resources, L.Z., S.C. and Y.W.; data curation, P.Z. and M.R.; writing—original draft preparation, D.J.; writing—review and editing, X.Y., Y.L., Z.Y., M.R., X.W.(Xinping Wang) and Y.W.; visualization, D.J. and Y.W.; supervision, X.W.(Xinping Wang), S.C. and Y.W.; project administration, S.C. and M.R.; funding acquisition, S.C. and Y.W.; All authors have read and agreed to the published version of the manuscript.

Funding: This work was supported by the Sichuan Province Science and Technology Planning Project (grant number 2021YFSY0005).

Institutional Review Board Statement: All animal experiments were approved by the institutional animal care and use committee of Sichuan Agricultural University of China (Approval number SYXK2019-187). All animal experiments were performed under the Laboratory Animals Welfare and Ethics published by the General Administration of Quality Supervision, Inspection and Quarantine of the People's Republic of China.

Informed Consent Statement: Not applicable.

Data Availability Statement: The data presented in this study are available on request from the corresponding author.

Conflicts of Interest: The authors declare that they are no conflict of interest.

References

1. Guo, Z.; Chen, X.; Li, R.; Qiao, S.; Zhang, G. The prevalent status and genetic diversity of porcine reproductive and respiratory syndrome virus in China: A molecular epidemiological perspective. *Virol. J.* **2018**, *15*, 2. [CrossRef] [PubMed]
2. Mateu, E.; Diaz, I. The challenge of PRRS immunology. *Vet. J.* **2008**, *177*, 345–351. [CrossRef] [PubMed]
3. Oie, A. *Manual of Diagnostic Tests and Vaccines for Terrestrial Animals*; Bulletin—Office International des Epizooties: Paris, France, 2015; pp. 1092–1106.
4. Brockmeier, S.L.; Loving, C.L.; Vorwald, A.C.; Kehrli, M.J.; Baker, R.B.; Nicholson, T.L.; Lager, K.M.; Miller, L.C.; Faaberg, K.S. Genomic sequence and virulence comparison of four Type 2 porcine reproductive and respiratory syndrome virus strains. *Virus Res.* **2012**, *169*, 212–221. [CrossRef]
5. Li, C.; Zhuang, J.; Wang, J.; Han, L.; Sun, Z.; Xiao, Y.; Ji, G.; Li, Y.; Tan, F.; Li, X.; et al. Outbreak Investigation of NADC30-Like PRRSV in South-East China. *Transbound. Emerg. Dis.* **2016**, *63*, 474–479. [CrossRef]
6. Tian, K. NADC30-Like Porcine Reproductive and Respiratory Syndrome in China. *Open Virol. J.* **2017**, *11*, 59–65. [CrossRef] [PubMed]

7. Sun, Y.F.; Yu, H.; Jiang, X.; Ma, J.F.; Xu, C.Q.; Yu, X.X.; Li, L.A. Novel ORF5 deletion of NADC30-like porcine reproductive and respiratory syndrome viruses circulating in northern China from 2016 to 2018. *J. Vet. Diagn. Investig.* **2020**, *32*, 928–932. [[CrossRef](#)] [[PubMed](#)]
8. Wang, H.M.; Liu, Y.G.; Tang, Y.D.; Liu, T.X.; Zheng, L.L.; Wang, T.Y.; Liu, S.G.; Wang, G.; Cai, X.H. A natural recombinant PRRSV between HP-PRRSV JXA1-like and NADC30-like strains. *Transbound. Emerg. Dis.* **2018**, *65*, 1078–1086. [[CrossRef](#)]
9. Bian, T.; Sun, Y.; Hao, M.; Zhou, L.; Ge, X.; Guo, X.; Han, J.; Yang, H. A recombinant type 2 porcine reproductive and respiratory syndrome virus between NADC30-like and a MLV-like: Genetic characterization and pathogenicity for piglets. *Infect. Genet. Evol.* **2017**, *54*, 279–286. [[CrossRef](#)]
10. Li, Y.; Ji, G.; Wang, J.; Tan, F.; Zhuang, J.; Li, X.; Tian, K. Complete Genome Sequence of an NADC30-Like Porcine Reproductive and Respiratory Syndrome Virus Characterized by Recombination with Other Strains. *Genome Announc.* **2016**, *4*, e00330-16. [[CrossRef](#)]
11. Li, X.; Bao, H.; Wang, Y.; Tian, K. Widespread of NADC30-like PRRSV in China: Another Pandora's box for Chinese pig industry as the outbreak of highly pathogenic PRRSV in 2006? *Infect. Genet. Evol.* **2017**, *49*, 12–13. [[CrossRef](#)]
12. Ding, Y.; Wubshet, A.K.; Ding, X.; Zhang, Z.; Li, Q.; Dai, J.; Hou, Q.; Hu, Y.; Zhang, J. Evaluation of Four Commercial Vaccines for the Protection of Piglets against the Highly Pathogenic Porcine Reproductive and Respiratory Syndrome Virus (hp-PRRSV) QH-08 Strain. *Vaccines* **2021**, *9*, 1020. [[CrossRef](#)] [[PubMed](#)]
13. Zhang, Q.; Jiang, P.; Song, Z.; Lv, L.; Li, L.; Bai, J. Pathogenicity and antigenicity of a novel NADC30-like strain of porcine reproductive and respiratory syndrome virus emerged in China. *Vet. Microbiol.* **2016**, *197*, 93–101. [[CrossRef](#)] [[PubMed](#)]
14. Leng, C.; Zhang, W.; Zhang, H.; Kan, Y.; Yao, L.; Zhai, H.; Li, M.; Li, Z.; Liu, C.; An, T.; et al. ORF1a of highly pathogenic PRRS attenuated vaccine virus plays a key role in neutralizing antibody induction in piglets and virus neutralization In Vitro. *Virol. J.* **2017**, *14*, 159. [[CrossRef](#)] [[PubMed](#)]
15. Wang, X.X.; Wang, F.X.; Li, Z.G.; Wen, Y.J.; Wang, X.; Song, N.; Wu, H. Development of an indirect enzyme-linked immunosorbent assay (ELISA) to differentiate antibodies against wild-type porcine reproductive and respiratory syndrome from the vaccine strain TJM-F92 based on a recombinant Nsp2 protein. *J. Virol. Methods* **2018**, *251*, 151–154. [[CrossRef](#)]
16. Liu, C.; Zhang, W.; Gong, W.; Zhang, D.; She, R.; Xu, B.; Ning, Y. Comparative Respiratory Pathogenicity and Dynamic Tissue Distribution of Chinese Highly Pathogenic Porcine Reproductive and Respiratory Syndrome Virus and its Attenuated Strain in Piglets. *J. Comp. Pathol.* **2015**, *153*, 38–49. [[CrossRef](#)]
17. Zhou, L.; Yang, B.; Xu, L.; Jin, H.; Ge, X.; Guo, X.; Han, J.; Yang, H. Efficacy evaluation of three modified-live virus vaccines against a strain of porcine reproductive and respiratory syndrome virus NADC30-like. *Vet. Microbiol.* **2017**, *207*, 108–116. [[CrossRef](#)]
18. Wei, Z.; Zhang, J.; Zhuang, J.; Sun, Z.; Gao, F.; Yuan, S. Immunization of pigs with a type 2 modified live PRRSV vaccine prevents the development of a deadly long lasting hyperpyrexia in a challenge study with highly pathogenic PRRSV JX143. *Vaccine* **2013**, *31*, 2062–2066. [[CrossRef](#)]
19. Li, T.; Peng, T. Traditional Chinese herbal medicine as a source of molecules with antiviral activity. *Antivir. Res.* **2013**, *97*, 1–9. [[CrossRef](#)]
20. Pan, M.H.; Chiou, Y.S.; Tsai, M.L.; Ho, C.T. Anti-inflammatory activity of traditional Chinese medicinal herbs. *J. Tradit. Complement. Med.* **2011**, *1*, 8–24. [[CrossRef](#)]
21. Zhou, W.; Zhang, X.Y. Research progress of Chinese herbal medicine Radix isatidis (banlangen). *Am. J. Chin. Med.* **2013**, *41*, 743–764. [[CrossRef](#)]
22. Ping, X.; Huang, H.; Chen, J.; Xiang, L. In Vitro antioxidant and anti-inflammatory activities of Radix Isatidis extract and bioaccessibility of six bioactive compounds after simulated gastro-intestinal digestion. *J. Ethnopharmacol.* **2014**, *157*, 55–61.
23. Wei, Z.Y.; Wang, X.B.; Zhang, H.Y.; Yang, C.H.; Wang, Y.B.; Xu, D.H.; Chen, H.Y.; Cui, B.A. Inhibitory effects of indigowoad root polysaccharides on porcine reproductive and respiratory syndrome virus replication In Vitro. *Antivir. Ther.* **2011**, *16*, 357–363. [[CrossRef](#)] [[PubMed](#)]
24. Wang, X.; Xue, Y.; Li, Y.; Liu, F.; Yan, Y.; Zhang, H.; Jin, Q. Effects of Isatis root polysaccharide in mice infected with H3N2 swine influenza virus. *Res. Vet. Sci.* **2018**, *119*, 91–98. [[CrossRef](#)] [[PubMed](#)]
25. Li, L.; Yao, H.; Li, X.; Zhang, Q.; Wu, X.; Wong, T.; Zheng, H.; Fung, H.; Yang, B.; Ma, D.; et al. Destiny of Dendrobium officinale Polysaccharide after Oral Administration: Indigestible and Nonabsorbing, Ends in Modulating Gut Microbiota. *J. Agric. Food Chem.* **2019**, *67*, 5968–5977. [[CrossRef](#)]
26. Fang, Q.; Hu, J.; Nie, Q.; Nie, S. Effects of polysaccharides on glycometabolism based on gut microbiota alteration. *Trends Food Sci. Technol.* **2019**, *92*, 65–70. [[CrossRef](#)]
27. Chen, R.; Liu, B.; Wang, X.; Chen, K.; Zhang, K.; Zhang, L.; Fei, C.; Wang, C.; Liu, Y.; Xue, F.; et al. Effects of polysaccharide from Pueraria lobata on gut microbiota in mice. *Int. J. Biol. Macromol.* **2020**, *158*, 740–749. [[CrossRef](#)]
28. Ghatak, A.; Chaturvedi, P.; Weckwerth, W. Cereal Crop Proteomics: Systemic Analysis of Crop Drought Stress Responses towards Marker-Assisted Selection Breeding. *Front. Plant Sci.* **2017**, *8*, 757. [[CrossRef](#)]
29. Meng, L.; Zhang, T.; Geng, S.; Scott, P.B.; Li, H.; Chen, S. Comparative proteomics and metabolomics of JAZ7-mediated drought tolerance in Arabidopsis. *J. Proteom.* **2019**, *196*, 81–91. [[CrossRef](#)]
30. Jiang, J.; Ren, X.; Li, L.; Hou, R.; Dong, Y. H2S Regulation of Metabolism in Cucumber in Response to Salt-Stress Through Transcriptome and Proteome Analysis. *Front. Plant Sci.* **2020**, *11*, 1283. [[CrossRef](#)]

31. Wang, L.; Zhang, Y.; Zhang, B.; Zhong, H.; Lu, Y.; Zhang, H. Candidate gene screening for lipid deposition using combined transcriptomic and proteomic data from Nanyang black pigs. *BMC Genom.* **2021**, *22*, 441. [[CrossRef](#)]
32. Dai, W.; Wang, Q.; Zhao, F.; Liu, J.; Liu, H. Understanding the regulatory mechanisms of milk production using integrative transcriptomic and proteomic analyses: Improving inefficient utilization of crop by-products as forage in dairy industry. *BMC Genom.* **2018**, *19*, 403. [[CrossRef](#)]
33. Cheng, X.Y.; Liu, X.Y.; Wang, H.M.; Su, C.T.; Zhao, R.; Bodelier, P.; Wang, W.Q.; Ma, L.Y.; Lu, X.L. USCgamma Dominated Community Composition and Cooccurrence Network of Methanotrophs and Bacteria in Subterranean Karst Caves. *Microbiol. Spectr.* **2021**, *9*, e00820-21. [[CrossRef](#)] [[PubMed](#)]
34. Lim, B.; Kim, S.; Lim, K.S.; Jeong, C.G.; Kim, S.C.; Lee, S.M.; Park, C.K.; Te, P.M.; Gho, H.; Kim, T.H.; et al. Integrated time-serial transcriptome networks reveal common innate and tissue-specific adaptive immune responses to PRRSV infection. *Vet. Res.* **2020**, *51*, 128. [[CrossRef](#)] [[PubMed](#)]
35. Lozupone, C.; Knight, R. UniFrac: A new phylogenetic method for comparing microbial communities. *Appl. Environ. Microbiol.* **2005**, *71*, 8228–8235. [[CrossRef](#)] [[PubMed](#)]
36. Kristiansen, H.; Gad, H.H.; Eskildsen-Larsen, S.; Despres, P.; Hartmann, R. The oligoadenylate synthetase family: An ancient protein family with multiple antiviral activities. *J. Interferon Cytokine Res.* **2011**, *31*, 41–47. [[CrossRef](#)]
37. Welch, S.K.; Calvert, J.G. A brief review of CD163 and its role in PRRSV infection. *Virus Res.* **2010**, *154*, 98–103. [[CrossRef](#)]
38. Van Gorp, H.; Van Breedam, W.; Delputte, P.L.; Nauwynck, H.J. Sialoadhesin and CD163 join forces during entry of the porcine reproductive and respiratory syndrome virus. *J. Gen. Virol.* **2008**, *89*, 2943–2953. [[CrossRef](#)]
39. Calvert, J.G.; Slade, D.E.; Shields, S.L.; Jolie, R.; Mannan, R.M.; Ankenbauer, R.G.; Welch, S.K. CD163 expression confers susceptibility to porcine reproductive and respiratory syndrome viruses. *J. Virol.* **2007**, *81*, 7371–7379. [[CrossRef](#)]
40. Du, T.; Nan, Y.; Xiao, S.; Zhao, Q.; Zhou, E.M. Antiviral Strategies against PRRSV Infection. *Trends Microbiol.* **2017**, *25*, 968–979. [[CrossRef](#)]
41. Li, Y.; Renner, D.M.; Comar, C.E.; Whelan, J.N.; Reyes, H.M.; Cardenas-Diaz, F.L.; Truitt, R.; Tan, L.H.; Dong, B.; Alysandratos, K.D.; et al. SARS-CoV-2 induces double-stranded RNA-mediated innate immune responses in respiratory epithelial-derived cells and cardiomyocytes. *Proc. Natl. Acad. Sci. USA* **2021**, *118*, e2022643118. [[CrossRef](#)]
42. Sola, I.; Almazan, F.; Zuniga, S.; Enjuanes, L. Continuous and Discontinuous RNA Synthesis in Coronaviruses. *Annu. Rev. Virol.* **2015**, *2*, 265–288. [[CrossRef](#)] [[PubMed](#)]
43. Bi, J.; Song, S.; Fang, L.; Wang, D.; Jing, H.; Gao, L.; Cai, Y.; Luo, R.; Chen, H.; Xiao, S. Porcine reproductive and respiratory syndrome virus induces IL-1beta production depending on TLR4/MyD88 pathway and NLRP3 inflammasome in primary porcine alveolar macrophages. *Mediat. Inflamm.* **2014**, *2014*, 403515. [[CrossRef](#)] [[PubMed](#)]
44. Wang, C.; Shi, X.; Zhang, X.; Wang, A.; Wang, L.; Chen, J.; Deng, R.; Zhang, G. The Endoribonuclease Activity Essential for the Nonstructural Protein 11 of Porcine Reproductive and Respiratory Syndrome Virus to Inhibit NLRP3 Inflammasome-Mediated IL-1beta Induction. *DNA Cell Biol.* **2015**, *34*, 728–735. [[CrossRef](#)] [[PubMed](#)]
45. Schroder, K.; Tschopp, J. The inflammasomes. *Cell* **2010**, *140*, 821–832. [[CrossRef](#)]
46. Atianand, M.K.; Rathinam, V.A.; Fitzgerald, K.A. Snapshot: Inflammasomes. *Cell* **2013**, *153*, 272–272.e1. [[CrossRef](#)]
47. Okamura, H.; Nagata, K.; Komatsu, T.; Tanimoto, T.; Nukata, Y.; Tanabe, F.; Akita, K.; Torigoe, K.; Okura, T.; Fukuda, S.; et al. A novel costimulatory factor for gamma interferon induction found in the livers of mice causes endotoxic shock. *Infect. Immun.* **1995**, *63*, 3966–3972. [[CrossRef](#)]
48. Larsen, J.M. The immune response to Prevotella bacteria in chronic inflammatory disease. *Immunology* **2017**, *151*, 363–374. [[CrossRef](#)]
49. Mutlu, E.A.; Keshavarzian, A.; Losurdo, J.; Swanson, G.; Siewe, B.; Forsyth, C.; French, A.; Demarais, P.; Sun, Y.; Koenig, L. A Compositional Look at the Human Gastrointestinal Microbiome and Immune Activation Parameters in HIV Infected Subjects. *PLoS Pathog.* **2014**, *10*, e1003829. [[CrossRef](#)]
50. Yang, L.; Poles, M.A.; Fisch, G.S.; Ma, Y.; Nossa, C.; Phelan, J.A.; Pei, Z. HIV-induced immunosuppression is associated with colonization of the proximal gut by environmental bacteria. *AIDS* **2016**, *30*, 19–29. [[CrossRef](#)]
51. Tian, Z.; Liu, Y.; Yang, B.; Zhang, J.; He, H.; Ge, H.; Wu, Y.; Shen, Z. Astagalus Polysaccharide Attenuates Murine Colitis through Inhibition of the NLRP3 Inflammasome. *Planta Med.* **2017**, *83*, 70–77. [[CrossRef](#)]
52. Li, E.; Sun, N.; Zhao, J.X.; Sun, Y.G.; Huang, J.G.; Lei, H.M.; Guo, J.H.; Hu, Y.L.; Wang, W.K.; Li, H.Q. In Vitro evaluation of antiviral activity of tea seed saponins against porcine reproductive and respiratory syndrome virus. *Antivir. Ther.* **2015**, *20*, 743–752. [[CrossRef](#)]
53. Mosmann, T. Rapid colorimetric assay for cellular growth and survival: Application to proliferation and cytotoxicity assays. *J. Immunol. Methods* **1983**, *65*, 55–63. [[CrossRef](#)]
54. Kim, D.; Langmead, B.; Salzberg, S.L. HISAT: A fast spliced aligner with low memory requirements. *Nat. Methods* **2015**, *12*, 357–360. [[CrossRef](#)]
55. Chen, S.; Zhou, Y.; Chen, Y.; Jia, G. Fastp: An ultra-fast all-in-one FASTQ preprocessor. *Bioinformatics* **2018**, *34*, 884–890. [[CrossRef](#)] [[PubMed](#)]
56. Trapnell, C.; Williams, B.A.; Pertea, G.; Mortazavi, A.; Kwan, G.; van Baren, M.J.; Salzberg, S.L.; Wold, B.J.; Pachter, L. Transcript assembly and quantification by RNA-Seq reveals unannotated transcripts and isoform switching during cell differentiation. *Nat. Biotechnol.* **2010**, *28*, 511–515. [[CrossRef](#)] [[PubMed](#)]

57. Li, Y.; Lin, B.; Yang, L. Comparative Transcriptomic Analysis of Multiple Cardiovascular Fates from Embryonic Stem Cells Predicts Novel Regulators in Human Cardiogenesis. *Sci. Rep.* **2015**, *5*, 9758. [[CrossRef](#)]
58. Trapnell, C.; Roberts, A.; Goff, L.; Pertea, G.; Kim, D.; Kelley, D.R.; Pimentel, H.; Salzberg, S.L.; Rinn, J.L.; Pachter, L. Differential gene and transcript expression analysis of RNA-seq experiments with TopHat and Cufflinks. *Nat. Protoc.* **2012**, *7*, 562–578. [[CrossRef](#)] [[PubMed](#)]
59. Livak, K.J.; Schmittgen, T.D. Analysis of relative gene expression data using real-time quantitative PCR and the 2^{(-Delta Delta C(T))} Method. *Methods* **2001**, *25*, 402–408. [[CrossRef](#)] [[PubMed](#)]
60. Jakoby, T.; van den Berg, B.H.; Tholey, A. Quantitative protease cleavage site profiling using tandem-mass-tag labeling and LC-MALDI-TOF/TOF MS/MS analysis. *J. Proteome Res.* **2012**, *11*, 1812–1820. [[CrossRef](#)] [[PubMed](#)]
61. Chen, X.; Liu, H.; Wang, S.; Zhang, C.; Liu, L.; Yang, M.; Zhang, J. Combined transcriptome and proteome analysis provides insights into anthocyanin accumulation in the leaves of red-leaved poplars. *Plant Mol. Biol.* **2021**, *106*, 491–503. [[CrossRef](#)]
62. Bolyen, E.; Rideout, J.R.; Dillon, M.R.; Bokulich, N.A.; Abnet, C.C.; Al-Ghalith, G.A.; Alexander, H.; Alm, E.J.; Arumugam, M.; Asnicar, F.; et al. Reproducible, interactive, scalable and extensible microbiome data science using QIIME 2. *Nat. Biotechnol.* **2019**, *37*, 852–857. [[CrossRef](#)] [[PubMed](#)]
63. Callahan, B.J.; McMurdie, P.J.; Rosen, M.J.; Han, A.W.; Johnson, A.J.; Holmes, S.P. DADA2: High-resolution sample inference from Illumina amplicon data. *Nat. Methods* **2016**, *13*, 581–583. [[CrossRef](#)] [[PubMed](#)]
64. Rosen, M.J.; Callahan, B.J.; Fisher, D.S.; Holmes, S.P. Denoising PCR-amplified metagenome data. *BMC Bioinform.* **2012**, *13*, 283. [[CrossRef](#)] [[PubMed](#)]
65. DeSantis, T.Z.; Hugenholtz, P.; Larsen, N.; Rojas, M.; Brodie, E.L.; Keller, K.; Huber, T.; Dalevi, D.; Hu, P.; Andersen, G.L. Greengenes, a chimera-checked 16S rRNA gene database and workbench compatible with ARB. *Appl. Environ. Microbiol.* **2006**, *72*, 5069–5072. [[CrossRef](#)]
66. Bokulich, N.A.; Kaehler, B.D.; Rideout, J.R.; Dillon, M.; Bolyen, E.; Knight, R.; Huttley, G.A.; Gregory, C.J. Optimizing taxonomic classification of marker-gene amplicon sequences with QIIME 2's q2-feature-classifier plugin. *Microbiome* **2018**, *6*, 90. [[CrossRef](#)]
67. Shannon, C.E. The mathematical theory of communication. 1963. *MD Comput.* **1997**, *14*, 306–317.
68. Simpson, E.H. Measurement of Diversity. *Nature* **1949**, *163*, 688. [[CrossRef](#)]
69. Chao, A. Nonparametric estimation of the number of classes in a population. *Scand. J. Statist.* **1984**, *11*, 265–270.
70. Yang, C.M.C.K. Stopping rules and estimation for recapture debugging with unequal failure rates. *Biometrika* **1993**, *80*, 193–201.
71. Faith, D.P. Conservation evaluation and phylogenetic diversity. *Biol. Conserv.* **1992**, *61*, 1–10. [[CrossRef](#)]
72. Pielou, E.C.J. The Measurement of Diversity in Different Types of Biological Collections. *J. Theor. Biol.* **1966**, *13*, 131–144. [[CrossRef](#)]
73. Good, I.J. The population frequencies of species and the estimation of population parameters. *Biometrika* **1953**, *40*, 237–264. [[CrossRef](#)]
74. Ramette, A. Multivariate analyses in microbial ecology. *FEMS Microbiol. Ecol.* **2007**, *62*, 142–160. [[CrossRef](#)] [[PubMed](#)]